Minimally invasive activation of spared interneurons alleviates local CA1 hypersynchrony and behavioral deficits in a model of temporal lobe epilepsy

Célanie Matringhen[1], Alexandre Vigier[1], Nikoleta Bourtouli[2], Thomas Marissal[1*]

Author affiliation:

[1] INMED, INSERM, Aix-Marseille University, France
[2] National and Kapodistrian University of Athens, Greece

*Corresponding author. Email address: thomas.marissal@inserm.fr

Abstract:

Background: Temporal lobe epilepsy (TLE) is associated with severe cognitive impairments including memory deficits. The dysfunction of hippocampal inhibitory neurons is proposed as a key mechanism and possible target for therapeutic approaches. However, the nature and extent of alterations in hippocampal inhibitory neurons remain unclear, as does their impact on behavioral impairments associated with TLE.

Methods: We investigated the role of inhibitory neurons from the CA1 hippocampal region on memory deficits associated with TLE, considering both the survival and changes in the activity of a large population of interneurons. To this end, we used a combination of immunolabelling, calcium imaging, electrophysiology, human-applicable chemogenetic tools, and behavioral testing on a reliable mouse pilocarpine TLE model.

Results: We show that in TLE mice with severely disturbed spatial behavior, CA1 major interneuron populations are spared from histological damages that affect the epileptic hippocampus (e.g., sclerosis). However, CA1 interneurons fire less in epileptic than in control conditions, resulting in increased synchronization and activity of the epileptic CA1 network in vitro. Restoring CA1 interneuron discharge using a chemogenetic strategy rescued CA1 activity and synchronization in vitro. In vivo, the minimally invasive chemogenetic activation of hippocampal interneurons does not affect generalized seizures but reduces behavioral alterations.

Conclusions: Our data suggest that rescuing CA1 local network dynamics using interneurons as a lever could be sufficient to decrease behavioral deficits related to TLE.

Keywords: Temporal lobe epilepsy; Behavioral alterations; Memory deficits; Hippocampus; Network dynamics; Interneurons.

Acknowledgement and disclosures:

The list of authors has been established in accordance with INSERM recommendations for the signature of scientific articles in the field of life and health sciences (https://pro.inserm.fr/rubriques/recherche-responsable/integrite-scientifique/signature-des-publications-scientifiques). The author contribution to the present project was the following: Célanie Matringhen: Conceptualization, Investigation, Formal analysis, Validation, Writing - Review & Editing; Alexandre Vigier: Investigation, Formal analysis, Methodology, Writing - Review & Editing; Nikoleta Bourtouli: Investigation, Formal analysis, Writing - Review & Editing Thomas Marissal: Conceptualization, Investigation, Formal analysis, Methodology, Validation, Resources, Writing - Original Draft, Visualization, Supervision, Project administration, Funding acquisition.

The authors have benefited from some resources and facilities hosted at the INMED as well as the teams of Valérie Crépel and Ede Rancz, where the project has been initiated and completed, respectively. The authors want to thank Emilie Pallesi, François J. Michel, Severine Pellegrino, Philippe Moudery, Céline Boileau, Catherine Faivre-Sarrailh, Charles Quairiaux, Pierre-Pascal Lenck-Santini, Elodie Fino for having led their respective facilities, contributed to student supervision, and/or provided technical or administrative help and useful discussions. This work was supported by the Institut National de la Santé et de la Recherche Médicale (INSERM), Aix-Marseille University (AMU), the Agence Nationale de la Recherche (ANR-17-NEU3-0003-02 and ANR-18-17CEL), the INSERM First Step program, the Foundation A*Midex (AMX-22-RE-AB-161), the Foundation Fyssen, the Neuroschool MSc incoming mobility program, the NeuroMarseille International Collaborative Research program (NM2MARIINM) the PHC-Germaine-de-Staël program and the Ligue Française contre l'Epilepsie (LFCE). This work has received support from the French government under the "France 2030" program via A*Midex (Initiative d'Excellence d'Aix-Marseille Université, AMX-19-IET-004) and ANR funding (ANR-17-EURE-002).

The authors report no biomedical financial interests or potential conflicts of interest.

Introduction:

Temporal lobe epilepsy (TLE) is associated with cognitive impairments, including memory deficits, which are considered by many patients to be at least as disabling as seizures (1). A proposed mechanism to explain these cognitive alterations is the perturbation of the hippocampal inhibitory microcircuits essential to proper behavioral computation (2). Pioneer observations performed using rat TLE models suggest that a subclass-specific hippocampal inhibitory neuron loss may occur during the early disease stages (3), when spatial memory deficits emerge (4). Notably, oriens-lacunosum-moleculare neurons (O-LM, that express Somatostatin, or SOM), and axo-axonic cells (that express Parvalbumin, or PV) appear vulnerable, while other types (e.g., PV basket cells) seem relatively preserved in the CA1 region from rat pilocarpine model (3,5). In similar models, surviving inhibitory neurons of the hippocampus exhibit a change in their morphological, intrinsic, and synaptic properties in TLE conditions, which sometimes lead to a modification of their discharge (5–10). These alterations are correlated with the modification of the inhibition received by the pyramidal neurons network (5), which may underly the perturbated network activity and impaired behavior (7). On this basis, several attempts have been made to determine whether targeting inhibitory neurons could alleviate TLE pathological traits. To replenish the pool of hippocampal interneurons, various strategies based on stem cell grafting or reactive glia reprogramming have been tested (11,12). However, the clinical application of these approaches remains questionable given that recent observations from patients and mouse models of TLE suggest that the loss of CA1 inhibitory neurons can be modest or absent, and unlikely to contribute to spatial coding deficits (13,14). Some other studies have tested the effect of specifically manipulating a single class of inhibitory neurons (e.g., PV neurons), using chemogenetic or optogenetic tools, sometimes combined with a closed-loop system with EEG monitoring. Again, apart from the difficulties of adaptation for patients in their current state, these strategies also face several limitations. Firstly, most are based on the excitation of a single class of inhibitory neurons postulated to be already hyperactive or hyperexcitable in epileptic conditions, and their effect on seizures (15–17) or behavioral alterations (18,19) is not always beneficial. Secondly, these studies overlook the extent of degeneration of the considered inhibitory neuron subtype, a factor that could nonetheless affect the effect of their manipulation. Lastly, these studies rarely take into account the complementary physiopathological role played by the different classes of inhibitory neurons (e.g., PV and SOM neurons)(20–24). These different interneuron subclasses form interconnected inhibitory microcircuits that control CA1 network dynamics (25), and their global

activation could control pathological activity more efficiently than stimulation of a single subpopulation (26).

To tackle all these issues and help craft an adequate therapeutical strategy, we have clarified the impact of CA1 inhibitory microcircuit dysfunction on the cognitive alterations associated with TLE, taking into account both the survival and changes in the activity of a large population of interneurons that includes PV and SOM cells. To this end, we used a combination of calcium imaging, electrophysiology and behavioral testing performed on reliable mouse pilocarpine TLE models (27–29), as well as minimally invasive neuronal manipulation strategies that are potentially applicable to humans. We show that in TLE mice with severely disturbed spatial behavior, CA1 interneurons are spared from histological damages that affect the epileptic hippocampus (e.g., sclerosis). However, CA1 interneurons fire less in epileptic than in control conditions, resulting in increased synchronization and activity of the epileptic CA1 network in vitro. Restoring CA1 interneuron discharge using a chemogenetic strategy rescued CA1 activity and synchronization in vitro. In vivo, the minimally invasive chemogenetic activation of hippocampal interneurons does not affect generalized seizures but alleviates behavioral alterations. Therefore, we propose that rescuing CA1 local network dynamics using interneurons as a lever could be sufficient to decrease behavioral deficits.

Methods and materials:

Animals

We used wild-type mice from Swiss/CD-1 backgrounds. Animals were kept on a normal 12h light/dark cycle at 22–24°C and with ad libitum access to food and water. Control and epileptic mice were single housed. All experiments conducted on mice were performed in accordance with the directives of European Community Council (2010/63/UE) and received approval from the French Ministry for Research, after ethical evaluation by the institutional animal care and use committee of Aix-Marseille University (APAFIS number: #23627).

Pilocarpine-based models of TLE

To study TLE at the neuronal, network, and behavioral levels, we used mouse pilocarpine-based models that reliably reproduce the alterations observed in patients. To examine the role of interneurons in cognitive comorbidities in vivo, we used a low-mortality pilocarpine-based procedure performed on 2-month-old males to generate mice that exhibit histological and electrophysiological characteristics associated with TLE (27). To investigate the relationship between the recruitment of interneurons and the CA1 epileptic network dynamics in vitro as in (28), we used long lifespan hippocampal organotypic slices prepared from animals of both sexes (referred to as “slices” for simplicity), which display, after administration of pilocarpine, histological and network dynamics alterations that are similar to those observed in tissues from patients with TLE (29,31).

Surgeries:

We performed surgery in some experimental groups of mice to inject AAVs and/or to record generalized ictal activity. In both casse, mice were subcutaneously injected with an analgesic (Buprenorphine, 45µg/kg) and an anti-inflammatory drug (Carprofene, 10mg/kg) 20-30 minutes prior to the surgery. Anesthesia was induced at 5% in a transparent chamber (Minerve) and maintained at 0.5–3% isoflurane (w/v) using a mouse gas mask (Minerve) in a stereotaxic apparatus (Stoelting Co.) coupled to a binocular microscope (SZ61, Olympus). Mice were maintained at 36.5–38°C using a heating pad and controlled via a rectal thermometer (Stoelting). Their heads were secured using ear bars, a jaw bar, and a nose clamp. Eyes were covered with ointment (Ocry-Gel). Lurocaïne (Lidocaine, 7mg/kg), a local analgesic, was injected below the skin overlaying the skull. Then, the two procedures differed:

- ***Viral injections:*** AAV constructs enabling the manipulation of inhibitory neurons using hM3D (AAV9-hDlx-GqDREADD-dTomato-Fishell-4)(32) were injected bilaterally in the dorsal and ventral hippocampi (coordinates: AP -1.8, ML ± 1, DV -2 and AP -3.3, ML ±2.3, DV -2.5 from the bregma, respectively) of control or chronically epileptic animals minimum 5 weeks after TLE induction. To this end, the scalp of the anesthetized animal was shaved using electric clippers and then incised using a scalpel blade. The skull bone was gently cleaned and dried. The position of the craniotomies was then defined with a fine marker. The skull was pierced using a dental driller (Fordedim), without damaging the meninges. Then, 500nL of AAV was injected using a Nanoject III injector (Drummond) and glass capillaries (rate: 20nL/seconds, 10 cycles separated by 1 second). After injections, the skin was sutured with surgical stitches (Ethilon 5-0 polyamide thread), then anesthesia was discontinued.
- ***Implantation of the EEG recording device:*** A minimum of two weeks after AAV injection, the scalp and one flank of the animal were shaved using electric clippers. The skin was cleaned with antiseptic (Vetadine) and sterile saline solution (0.9%, Osalia). The skull was exposed using a scalpel blade. Three craniotomies were made using a drill (Foredom): two in an intermediate position between the two AAV injection sites in both hemispheres (approximately AP -2.55 mm, ML +1.65 mm relative to Bregma), the last above the cerebellum as in (29). Then, the mouse flank was incised, and a subcutaneous pouch was created by blunt dissection. A radio-frequency transmitter (ETA-F10, DSI) was implanted inside the pocket close to the ventral abdominal region, with wires oriented towards the head. The two emitter wires were carefully slipped underneath the mouse's neck skin. The tip of the first wire was inserted into the hole above the right hippocampus (~2mm from skull surface). The second wire, placed above the cerebellum (~2 mm from the skull surface), served as the ground electrode. To fix the wires, a screw was put in each of the three holes and covered with dental cement (Paladur). Finally, the cranial and flank incisions were sutured using 5-0 polyamide filaments (Ethilon, Ethicon). Mice were injected with saline solution (0.9%, 0.35mL) and allowed to recover from the surgery on a heating pad until fully awakened. Animal weight was then monitored. Buprenorphine (45µg/kg) was injected 24 hours after surgery, and Carprofen (10mg/kg) and saline solution (0.9%, 0.35mL) were injected 24 and 48 hours after surgery, all subcutaneously.

Behavioral testing

We performed various tests to measure mouse behavior in different experimental conditions: pilocarpine-treated chronically epileptic animals two months after pilocarpine-based TLE induction (referred to as "Pilo") and age-matched controls, injected or not with AAVs, with normal drinking water, drinking water with 4% of sucrose (a condition referred to as "vehicle" or VEH), or CNO diluted in the 4%-sucrose drinking water (5mg/200ml). The administration of CNO or VEH lasted from the week preceding the behavior test to its completion. The administration of CNO in water is a less invasive method than daily intraperitoneal injections (33). The sucrose was used to cover the taste of CNO, which is postulated to be slightly bitter (34). Drinking water consumption was measured regularly to calculate the average CNO intake per animal per day. Before behavioral testing, mice were handled every day for a week, and habituated to the experimental room. Tests were performed under indirect room lighting condition and at similar times of the day difference due to circadian effects (i.e., starting from 10:00AM). Mouse behavior was continuously videotaped by a video camera placed above the apparatus, tracked using the Ethovision 11.5 software, and manually corrected if necessary.

- ***Barnes circular maze (BCM)*** (35): The apparatus consisted of an elevated circular platform made of metal (diameter = 100 cm; elevation from the ground = 90 cm, color: grey) containing 20 holes equally spaced around the periphery (diameter = 4 cm)(**Figure 1A, B**). Under one hole was placed a magnetic escape room (black) in which mice could hide. Under the remaining 19 holes were placed black caps, which, from the surface of the platform, appeared indistinguishable from the escape room. Distal visual cues (length/width = 30 cm) surrounded the platform. BCM was performed while a loudspeaker played 90 dB of white noise. 24h prior to the test, mice were allowed to freely explore the maze during 1-2 habituation

sessions of 3 minutes after which they were guided to the escape room. Then, mice underwent the acquisition phase of the test (during which spatial learning-related abilities were assessed). This acquisition phase consisted of 2 trials per day for 4 consecutive days during which the position of the escape room remained constant. For each trial, mice were placed in a start chamber in the middle of the maze. After 15 seconds, the chamber was lifted, and the animals were allowed to explore the maze. The trial concluded when the mice entered the escape room, or 2 minutes elapsed. If a mouse failed to enter the escape room within the 2-minute period, it was gently guided to the escape room by the operator and left there for 15 seconds prior to removal. For each day, several parameters were quantified to assess mouse performance, including: the success and failure rate (i.e., the % of mice per experimental group that identified or not the escape room location at least once per day of acquisition), the latency to locate the escape room (primary latency), along with the number of incorrect holes checked prior to finding the escape room or the completion of the test ("primary errors"). We discriminated between mice that made no or few errors during a session before identifying the escape room and mice that made no or few errors without identifying the escape room, and explored the arena very little (e.g., 0-3 holes explored, locomotion <100 cm) (**Figure S1A and S3A**). For quantification of primary latencies and errors, we calculated the average of the non-null values for each trial per day of the BCM acquisition phase. We also classified the mouse exploration strategy as direct (when mice found the escape room after less than 3 primary errors), serial (when mice spent the majority of the time on the periphery performing systematic hole searches in a clockwise or counterclockwise manner) or random (when mice ran circularly on the periphery with no or few hole inspections, failed to identify the escape chamber, jumped off the apparatus or poorly explored the apparatus during the duration of a trial)(35). In cases where the mouse used different explorations during the two same-day trials of the BCM acquisition phase, we selected for quantification the strategy that best reflected the use of visuospatial cues (i.e., direct rather than serial strategy and serial rather than random strategy) (37). To assess behaviors related to spatial memory, animals underwent the probe trial 72 hours after the last acquisition day. During the probe trial, the escape room was removed and replaced by a false escape box (identical to the cap placed underneath the other 19 holes). The probe trial was performed in similarly to the acquisition trials (15 seconds in the start chamber, 2 minutes of free exploration). The success rate, the latency prior to reaching to previous escape room location, the number of incorrect hole checks, and exploration strategies were measured, along with the time spent in the quadrant where the escape room was localized ("target zone"). We measured the distance covered by the mice (which gives an indication of locomotory activity) only during the BCM probe trial, which is the only stage of the test during which the animals remained on the apparatus for the same amount of time, except when epileptic mice jump off the apparatus (which we reported in **Figure S3A**). Given the extent and variability in the altered BCM-related behavior of epileptic mice, and in order to avoid missing values (e.g., no latency value in mice failing to find the escape room location), we performed a min-max normalization for latency and number of primary errors, as well as time in the target area, where a score of 0 is assigned to the best possible performance (e.g., the mouse quickly finds the escape room without making any errors during the acquisition phase, or stays the whole time in the target zone during the probe trial) and 1 to the worst possible performance (e.g., the mouse finds do not find the escape room, or just before the end of the test, or makes the maximum number of errors recorded, or jumps off the apparatus or doesn't explore any holes). The original data is shown in **Figure S1A and S3A**.

- ***Elevated plus maze (EPM)*** was performed to measure mouse anxiety (36)(**Figure S1C**). The apparatus consists of a grey-plexiglass-made plus-shaped maze, elevated 60cm above the floor, with a center area, two oppositely positioned closed arms (35x6 cm, surrounded by 15 cm-high walls) and two oppositely positioned open arms (35×6 cm). The test was initiated by placing the mouse in the center area of the maze, facing one of the open arms. Mice were allowed to explore the maze for 5 minutes and the time spent in each zone (open arms, closed arms) was measured, as well as the distance traveled during the test.
- ***Novel Object Recognition test (NORT)*** was performed to measure mouse non-spatial memory (37)(**Figure 4I**), which involves the dorsal CA1 (38). NORT was performed in a black

Plexiglas box (40 cm L x 40 cm W x 40 cm H). After habituation to the arena (10 minutes, 1 day prior to the test familiarization stage), mice were placed into the center of the box, in which two identical objects were placed in opposite quarters. During this familiarization stage, the time exploring each object was measured for 5 minutes using the Ethovision 11.5 software, then this value was checked and corrected, if necessary. Mouse were defined as exploring the object when they directed the nose at a distance of < 2 cm to the object. We have excluded mice that remained for >100 seconds in a quarter of the apparatus without exploratory behavior. One day later, during the testing phase, one of the objects was replaced by a new item of similar size, and the time exploring the familiar versus the novel object was measured for 5 minutes. To limit bias due to an animal's preference for a particular location in the apparatus, the new object was systematically placed at the location of the object least explored in the previous phase. The used objects included brick toys, blue and green 0.5L bottles, and needle boxes.

Histology

Mice were anesthetized (using a mix of Domitor 1.2mg/kg and Zoletil 80mg/kg) prior to intracardiac injection with PBS/heparin (0.1%) solution and then with 4%-paraformaldehyde-based solution (Antigenfix). Next, the animals were decapitated, and the brains were kept for a maximum of 24 h in Antigenfix at 4 ◦C and washed in PBS. Brains were placed overnight in 30% sucrose at 4◦C for cryopreservation. Afterward, brains were embedded in blocks containing optimum cutting temperature medium (OCT; Tissue-Tek) placed on dry ice, enabling tissue storage at 80◦C for months if necessary. Finally, coronal sections (60-µm-thick sections) were prepared at -25°C from the brain tissue blocks using a Cryostat (Leica CM3050S). Sections were stored in 24 well plates according to their position in the anteroposterior axis of the brain at 4°C in PBS-Azide (0.01%) until immunochemistry was performed. To enable subsequent comparison between conditions, we systematically selected for each animal two sections that are situated at 840 and 1200 µm posterior to the most anterior part of the hippocampus. These sections were permeabilized with PBS-Triton (1%) containing horse serum (10%) for 2 h at room temperature. Next, sections were incubated with polyclonal goat primary antibody directed against PV (Swant, 1:1000) or mouse anti-SOM (Santa-Cruz, 1:200) in PBS-Triton (1%) containing horse serum (10%) for 2 days at 4 ◦C under agitation. Sections were then washed with PBS, placed in PBS containing polyclonal donkey secondary antibody coupled with Alexa488 directed against goat (Invitrogen 1:500) and donkey secondary antibody coupled with Alexa647 directed against mouse (Invitrogen 1:500) for 2 h, and stained with Hoechst (1:2000, Sigma). Images were acquired using a confocal microscope (LSM800, Zeiss equipped with 10x/0.3 and 20×/0.3 objectives). Low magnification images of the Hoechst-stained dorsal hippocampus were acquired to assess for TLE-related histological damages (e.g., sclerosis). Then, immunofluorescence was detected in a field of X638.9 × Y638.9 µm (Z = 8 images, interval 2 µm) covering all sublayers of dorsal CA1 from the alveus to the stratum lacunosum-moleculare (see Figure 1). Images were processed and quantification was performed using ImageJ software. In brief, PV and SOM interneuron density per animal was estimated by dividing the average number of somata expressing PV or SOM by the area of CA1 from 4 images, 2 for each hemisphere.

Calcium imaging and analysis

To monitor the activity of a large population of CA1 neurons, slices were transduced with AAV constructs enabling the expression of the genetically encoded calcium sensor jGCaMP8m under the control of the human synapsin promoter (pGP-AAV-syn-jGCaMP8m-WPRE, AAV9, titer > 1×10^{13} vg/mL). pGP-AAV-syn-jGCaMP8m-WPRE was a gift from GENIE Project (Addgene, 162378-AAV9) (39). To identify and manipulate CA1 interneurons, slices were transduced with AAV constructs enabling the expression of the excitatory chemogenetic “DREADD” receptor hM3D and the red reporter dTomato under the control of the interneuron-specific hDlx enhancer element (pAAV-hDlx-GqDREADD-dTomato-Fishell-4, AAV9, titer >

7×10^{12} vg/mL)(32). pAAV-hDlx-GqDREADD-dTomato-Fishell-4 was a gift from Gordon Fishell (Addgene, 162375-AAV9 Addgene) (32). On the in vitro day 1 (DIV1), 300 nl of viral serum was applied above the hippocampus. 10-14 days later, slices were immersed in an artificial cerebrospinal fluid (ACSF) containing (in mM): 126 NaCl, 3.5 KCl, 1.2 NaH 2PO4, 26 NaHCO 3, 1.3 MgCl2, 2.0 CaCl2, and 10 glucose (pH ~7.4), continuously oxygenated and perfused at ~30 ◦C using a peristaltic pump. All compounds used for the preparation of the ACSF were purchased from Sigma-Aldrich.

Calcium transients were recorded using a multibeam two-photon laser scanning system (TriMScope, LaVision Biotec) mounted on a BX51WI Olympus microscope coupled to an Ultra II chameleon laser (Coherent). A fluorescent lamp (Olympus U-RFL-T) was used to identify a CA1 field with GCaMP-expressing neurons and dTomato-expressing interneurons. Slices were imaged using a 20 X 0.95NA objective (Olympus) at a ~23 Hz frame rate (i.e., 44 ms per frame) for up to ~7 minutes (i.e., 10,000 frames). The two-photon excitation wavelength was 920 nm. A typical imaging session covered a field of 300 × 150 µm size containing up to 100 individual CA1 neurons. To record the population activity in control versus pathological conditions as in (40,41), GCaMP-based calcium activity was recorded under the continuous presence of carbachol (Cch, Sigma). The application of Cch on hippocampal slices in vitro notably induces oscillatory activity resembling those that occur in vivo during navigation, learning and memory processes (40–42). To test the effect of interneuron manipulation on the network dynamics, some slices were monitored twice, the first time in Cch only, then the DREADD ligand clozapine-N-oxide (CNO, Tocris, 2µM) was applied in the bath in addition to the Cch for at least 15 minutes, followed by a second calcium imaging of the same slice. The detection of neurons and calcium activity onsets/offsets was performed semi-automatically in each movie using the Matlab-based 'Caltracer' software (Columbia University). Then, we calculated the levels of calcium activity (i.e., number of active neurons, frequency, amplitude, and duration of calcium transients), and quantified neuronal synchronization as in (28,41).

EEG recordings and analysis:

We performed EEG recordings to measure seizure activity in epileptic mice injected with AAV9-hDlx-GqDREADD-dTomato-Fishell-4 before and after chemo-activation of hippocampal interneurons (using CNO). On average 15 weeks after TLE induction and the week following surgery, individual cages containing implanted animals were placed on telemetric receiver plates, and EEG signals (1000× amplified, filtered at 0.16–97 Hz pass, and acquired at 500 Hz) were monitored 24 hours per day for minimum 7 consecutive days, while animals were administered a vehicle (i.e., 4% sucrose in the drinking water, ad libitum, for 5 days), then CNO (5mg in 200ml of 4% sucrose drinking water, ad libitum, for 2-5 days). The long duration of recordings was justified by the previous observation that spontaneous ictal events occur in clusters that can be separated by long seizure-free periods (27,43). Drinking water consumption was measured regularly to calculate the average CNO intake per animal per day.

EEG was analyzed using the Neuroscore software (DSI). EEG raw signal was visually inspected and the 'periodogram' function of DSI (time-frequency spectrogram of EEG, determined using a Fast Fourier Transform algorithm with a sliding 1 second-Hanning window) was used to help detect ictal events. Similar to (27,29), we quantified in each experimental conditions the frequency and duration of stereotyped tonic-clonic ictal activity characterized by rhythmic (4-60Hz) and prolonged (>10s) spike trains with an amplitude exceeding twice the baseline level. To limit the potential effect of anesthesia and post-surgical care (see Surgery section above), we only analyzed EEG signals recorded from the third day after implantation as in (44).

Statistical methods

For the comparison of multiple groups of two factors, we used the two-way ANOVA test followed by Sidak's post-hoc test when appropriate. For comparisons between two unpaired

groups with normal distribution, the two-tailed Student's t-test was used. For comparisons between two unpaired groups without normal distribution, the two-tailed Mann-Whitney test was used. For comparisons between two paired groups with normal distribution, the two-tailed paired t-test was used. For comparisons between two paired groups without normal distribution, the two-tailed Wilcoxon test was used. Normality was assessed using the Shapiro-Wilk test. For the analysis of categorical outcomes (e.g., success or failure), we used Fisher's exact test. All statistical tests were performed using GraphPad Prism Software and detailed in the figure legends.

Results

Impaired behavior in epileptic mice is not correlated with the loss of CA1 inhibitory neurons

Could a loss of CA1 inhibitory neurons explain cognitive deficits in epileptic mice? To answer this question, we investigated spatial memory in non-epileptic control and epileptic mice using BCM (see **Methods and Materials**, **Figure 1A-E, Figure S1A**). Under control conditions, 100% of the group of non-epileptic mice (referred to as "Controls") found the location of the escape room from day 1 to day 4 of the Barnes Circular Maze (BCM) acquisition phase and during the probe trial (PT) on day 7 (**Figure 1A-B**). By contrast, the behavioral pattern was very different for the group of pilocarpine-treated chronically epileptic animals (referred to as "Pilo"): only 61.5 % of the mice found the escape room on day 1, and this proportion did not significantly change after 4 days of acquisition (76.9% of mice found the escape room at least once during the four days of acquisition phase, **Figure 1A,** Fisher's exact test $p = 0.6728$). During the probe trial, only 69% of epileptic mice found the prior escape room location (**Figure 1B**).

We also compared the latency to find the escape room location, the number of primary errors during the BCM, as well as the time in the target zone during the PT between Controls and Pilo mice. To this end, we calculated for each parameter a min-max score where 0 is assigned to the best possible performance and 1 to the worst possible performance (**Methods and Material**, **Figure 1C-E** and **Figure S1A** for original data). Thus, the latency of control mice to find the escape room location diminished with time (**Figure S1A**), which is reflected by a significant decrease in the average min-max score between Day 1 and PT (Two-way repeated measures ANOVA days of acquisition $F (2.720, 89.77) = 6.104$ $p = 0.0012$ followed by Sidak's post hoc test, $p = 0.0012$ between D1 and PT, **Figure 1C**). By contrast, the scores related to the latency to find the escape room location were significantly higher in Pilo mice (**Figure 1C** and **S1A**). Similarly, Pilo mice displayed higher scores related to the number of errors made during the acquisition phase and PT (**Figure 1D**) and time in the target zone during the PT (**Figure 1E**) than Controls. A substantial proportion of control mice (>40%) used a direct exploration strategy while most epileptic mice explored the BCM randomly (**Figure S1B**). Therefore, our results suggest impaired behavior in epileptic mice undergoing a test measuring spatial learning and memory. The difference between controls and epileptic animals was not likely to be caused by an increase in anxiety in pilocarpine-treated animals given that time spent in the EPM open and closed arms was not significantly different between groups (**Figure S1C, D**). In addition, we observed no significant difference in mean distance traveled between control and pilocarpine mice during BCM probe trial or EPM (**Figure S1E**). More interestingly, we tested whether poor spatial behavior could be explained by the loss of major subclasses of CA1 inhibitory neurons, which were found degenerating in some TLE models (3). To this end, we collected the brains of some control and epileptic mice after they had undergone BCM, and immunolabeled neurons expressing PV and SOM (**Figure 1F**). Even though epileptic mice displayed histological changes similar to TLE patients (e.g., hippocampal sclerosis, **Figure S1F**), neither the density of PV nor SOM neurons was significantly different from controls (**Figure 1G-H**).

In line with (13), our results suggest that epileptic mice display altered behavior related to spatial learning and memory, which is not correlated with the loss of CA1 interneurons.

Hyper-synchronization of epileptic CA1 network is correlated with hypoactive inhibitory neurons and is reversible

Could an alteration in the discharge of spared CA1 inhibitory neurons play a role in TLE-relative memory defects? Despite numerous studies based on different models, it is still unclear whether the different categories of CA1 inhibitory neurons are hyperactive or "dormant", and whether their activation could produce a positive or negative effect on the pathological traits associated with TLE (21). To tackle this issue, we monitored the activity of a large number of CA1 neurons using in vitro GCaMP8m-based calcium imaging as in (41), in control slices versus pilocarpine-based TLE slices that exhibit physiological and histological alterations similar to those observed in hippocampal tissues from adult TLE patients (29,31)(**Figure 2A-E**). While the number of active cells was similar between both conditions (**Figure 2F**), CA1 neuron calcium activity was more frequent and synchronous in epileptic conditions than in control slices, which is reflected by significantly higher values in the frequency of calcium transients (**Figure 2G**), the number of coactive neurons (**Figure 2H**) as well as the occurrence of these neuronal coactivations (**Figure 2I**). We reported no difference between experimental groups in the average amplitude and duration of calcium transients (**Figure S2A-B**).

We also specifically recorded the GCaMP8m-based activity of dTomato-labeled Dlx-expressing population of interneurons that includes PV and SOM cells (see **Methods and Materials** and **Figure 2J-M**). In line with our in vivo data (**Figure 1F-H**), the number of interneurons per calcium imaging field was not different between control and epileptic conditions (**Figure 2K**). By contrast, the average frequency of calcium transients generated by CA1 interneurons was significantly smaller under epileptic conditions (**Figure 2L, M**). In conclusion, our data suggest that while the CA1 neuronal network is more active and synchronous, interneurons discharge significantly less in epileptic conditions compared to control slices.

Could a chemogenetic strategy targeting interneurons restore the activity of CA1 interneurons and re-establish the correct network dynamics? To test this, we compared the in vitro calcium activity in the epileptic CA1 neuronal network, including a few dTomato- and hM3D-expressing interneurons, before ('Pilo-VEH') and after 15 minutes of bath application of CNO (2 µM, see **Methods and materials**). The activation of the excitatory DREADD hM3D using CNO significantly increased the frequency of calcium transient generated by inhibitory neurons (**Figure 3A-B**), to levels that are comparable to the controls (unpaired t-test p = 0.3817, **Figure 2J-L**).

The chemogenic elevation of CA1 interneuron discharge attenuated the CA1 network activity (**Figure 3C**), which was reflected by a significant decrease in the percentage of active cells (**Figure 3D**) and average frequency of calcium transients generated all neurons of the imaged fields (**Figure 3E**). The level of CA1 network synchronization was also diminished by the interneuron manipulation, with a significant reduction of the number of neurons involved in coactivations, and the occurrence of these coactivations (**Figure 3F-G**) to levels that are similar to the controls (Mann-Whitney test p = 0.4084 for the number of coactive neurons and 0.1023 for the occurrence of coactivations, **Figure 2 H-I**). By contrast, the chemoactivation of hippocampal interneurons affected neither the amplitude nor the duration of calcium transient (**Figure S2C-D**). Therefore, our data suggest that rescuing interneuron firing is sufficient to restore local CA1 network dynamics *in vitro*.

The chemoactivation of hippocampal interneuron attenuates behavioral deficits, but not generalized seizures

Could the chemogenetic stimulation of hippocampal interneuron activity decrease the pathological traits associated with TLE, such as seizures and cognitive deficits?

To answer this question, we first performed in vivo EEG recordings on pilocarpine-treated TLE animals, in the hippocampus distant from injection sites, while hM3D-expressing

hippocampal interneurons were selectively activated through the presence of CNO in the drinking water (pilo-CNO condition), or not (pilo-VEH condition, (see **Methods and materials**). As expected, prolonged ictal activity reminiscent of generalized tonic-clonic seizures has been monitored in all pilocarpine-treated animals in the hippocampal region distant from injection sites (see **Methods and materials**, **Figure 4A**). Despite its impact on local synchronization in vitro (**Figure 2**), we observed no significant difference on the frequency and duration of generalized seizures between Pilo-VEH and Pilo-CNO conditions (**Figure 4B, C**). Mouse daily consumption of CNO via drinking water was estimated to 6mg/kg per day.

In parallel, we performed behavioral testing on pilocarpine-treated TLE animals with or without chemoactivation of hippocampal interneurons. We first used the BCM to assess behavior related to spatial learning and memory in epileptic mice while hM3D-expressing hippocampal interneurons were selectively activated through the presence of CNO in the drinking water (i.e., Pilo-CNO condition), or not (Pilo-VEH condition). We also used a group of vehicle-treated non-epileptic control mice (Control-VEHs).

In line with our data shown in **Figure 1**, animals in the pilo-VEH group show impaired behavior compared to Control-VEH mice (**Figure 4D-H** and **S3A-B**). While all Control-VEHs found the escape room on day 1 of the acquisition phase, a significantly lower number of pilo-VEHs identified the location of the escape room at this stage (60.9%), and this proportion did not change significantly after 4 days (78.3% of pilo-VEH mice found the escape room at least once during the 4 days of acquisition phase) (**Figure 4D**). Pilo-VEH success rate remained significantly lower than Control-VEHs during the PT (**Figure 4E**). In addition, the min-max scores related to the latency to locate the escape room (**Figure 4F**), the number of primary errors (**Figure 4G**), and the time in the target zone (**Figure 4H**) were significantly higher in Pilo-VEH than Control-VEH at any BCM stage (acquisition days 1-4 and PT). Last, Pilo-VEH exhibited significantly less direct exploration strategy than Control-VEHs at any BCM stages (**Figure S3B**).

On the contrary, epileptic mice treated with CNO, which display a different behavior from Control-VEH at the beginning of the BCM (e.g., acquisition day 1), no longer exhibit any significant difference during the later phases of the test (e.g., acquisition day 4 and PT) regarding success rate, latency, number of errors, and time in the target zone (**Figure 4D-H**). Notably, Pilo-CNO mice significantly increased cumulated success rate to reach 100% after 4 days of acquisition as in Control-VEH mice (**Figure 4D**) and the score related to the time in the target zone during PT significantly decreased to levels comparable with the Control-VEHs (**Figure 4H**). Similarly, the percentage of direct strategies used by Pilo-VEH mice is not significantly different from Control-VEH during the PT (**Figure S3B**).

In brief, the performance of TLE mice using a test measuring learning and spatial memory appeared slightly improved towards control values in conditions where hippocampal interneurons were stimulated, despite the persistence of seizures. To test whether other types of memory that are altered in TLE can also be rescued, we conducted NORT on all experimental groups (see **Methods and materials, Figure 4I**). During the familiarization phase, no experimental group showed a preference for either of the two identical objects (**Figure S3C**). During the test phase, the control mice explored the novel object significantly more than the familiar object while epileptic mice spent a similar amount of time exploring the two objects in the absence of interneuron manipulation, as expected (45) (**Figure 4J**). This suggests that behavior related to non-spatial memory is impaired in chronically epileptic animals. By contrast, preference for the novel object was rescued in Pilo-CNO animals (**Figure 4J**).

Regarding locomotory activity, we observed no significant group differences in the distance covered during the BCM probe trial, or the NORT familiarization and test phases, despite a general tendency for Pilo-VEHs to travel a shorter distance than Control-VEHs (**Figure S3D**).

Altogether, our data suggests that chemogenetic elevation of hippocampal interneuron discharge does not affect generalized seizures, but reduces the impairment of behaviors associated with learning and memory in epileptic mice.

Discussion:

Using behavioral testing followed by immunohistological analysis, we show pilocarpine-treated mouse model of TLE displays severe behavioral alterations related to spatial learning and memory, which is not correlated with a decrease in the density of CA1 interneurons expressing Parvalbumin or Somatostatin. Although in contradiction with observations in the epileptic rat (3,5), these data are in agreement with recent studies using the mouse pilocarpine model showing that spatial processing impairment is not correlated to a loss of CA1 interneuron (13). In contrast, our in vitro calcium imaging data suggest that under epileptic conditions, CA1 interneurons are hypoactive, while the neural network is excessively active and synchronous compared to the control. This observation brings new insight to the debate as to whether hippocampal interneurons are less active ("dormant") or rather hyperactive, thus justifying or not the use of strategies aimed at elevating their discharge (5,9,21,46–48).

We have not attempted to investigate the mechanisms that explain the reduced discharge of the Dlx-expressing population of CA1 interneurons, which include various morpho-physiological subtypes (32). Several studies suggest that the intrinsic and synaptic properties of certain inhibitory neurons may be altered under epileptic conditions, thereby modifying their firing (6,9). Instead of exploring the causes of interneuron dysfunction, we used a chemogenetic strategy potentially that does not rely on the Cre-Lox system and is applicable to humans to specifically restore their discharge (32). This interneuron-specific manipulation restores the activity and synchronization of the CA1 neuronal network in vitro to levels similar to the control. In vivo, the chemoactivation of interneurons did not reduce the tonic-clonic seizures recorded at a distance from the virus injection sites. This suggests that hippocampal interneuron manipulation restores network dynamics locally but does not prevent the emergence of generalized ictal activities, which involve a broader network of brain structures (49). In spite of the persistence of seizures, chemoactivation of interneurons significantly reduced cognitive impairments measured by tests related to spatial and non-spatial learning and memory.

Rodent models of TLE are thought to display locomotor alterations and anxiety-like behavior (50) that could disturb their cognitive performance, notably learning and memory processes. However, in our study, the poor performance of epileptic mice performing the BCM is not correlated with significant differences in the distance covered during the test (which reflects locomotion), or in the time spent in one of the EPM arms (which reflects anxiety) compared to controls. In addition, the chemoactivation of interneurons of hippocampal interneurons was sufficient to reduce the behavioral alterations displayed by epileptic mice performing BCM or NORT, two tests related to different forms of memory, without significantly modifying the average distance travelled. Therefore, we believe that the effect of interneuron manipulation on BCM and NORT performance is more likely explained by the rescue of the memory coding in CA1 (4,13,51) rather than by a compensatory mechanism involving the CA1 circuits regulating locomotion (52) or anxiety (53).

We focused on the CA1 region of the hippocampus, which is considered an important node in TLE. Highly susceptible to histological damages, CA1 could not only be involved in seizure generation and propagation (54–56), but also in the cognitive alterations associated with TLE (4,13,51), which drastically impair the patients' quality of life (1,57). In addition, the inhibitory microcircuits have been particularly well described in CA1 region under physiological (58) and pathological conditions (3,5,6,8,21,59).

Most, if not all, studies focusing on the role of inhibitory neurons in TLE are based on transgenic lines expressing a recombinase under the control of a specific promoter (i.e., PV-Cre), but also sometimes on heavy surgery to implant optical fibers for photostimulation, combined or not with an EEG device for close-loop seizure detection (15,16). In this study, we attempted to use a controllable and minimally invasive approach that could potentially be applied to patients with TLE. We used a method based on AAV vectors and the AAV regulatory sequence to restrict DREADD expression to interneurons. This method is effective in all non-genetically tractable vertebrate species, including humans (32). The genetic modification of the hippocampus in an intractable adult patient, which would be otherwise surgically removed

as last resort, is not out of the question in terms of ethics and biosafety (60,61). In addition, we used a drinking water-based method of DREADD ligand delivery, a technique reputed to be less invasive and stressful than intra-peritoneal injections or the use of mini-pumps (33). In vivo, our rescue strategy does not significantly reduce tonic-clonic seizure activity, but alleviates behavioral impairment related to learning and memory. This differential effect is consistent with the existence of distinct neuronal populations in the epileptic hippocampus, some participating in pathological activities, others regulating functional processes (62) that are perturbated in TLE (4,13,51). A possible therapeutical strategy to treat the different pathological traits of TLE would be to specifically target the hyperactive circuits to prevent seizure (29,63), whereas cognitive processes could be re-established by the manipulation of hippocampal interneurons.

Reference List:

1. Holmes GL (2013): EEG abnormalities as a biomarker for cognitive comorbidities in pharmacoresistant epilepsy. *Epilepsia* 54: 60–62.
2. Royer S, Zemelman BV, Losonczy A, Kim J, Chance F, Magee JC, Buzsáki G (2012): Control of timing, rate and bursts of hippocampal place cells by dendritic and somatic inhibition. *Nature Neuroscience* 15: 769–775.
3. Dinocourt C, Petanjek Z, Freund TF, Ben-Ari Y, Esclapez M (2003): Loss of interneurons innervating pyramidal cell dendrites and axon initial segments in the CA1 region of the hippocampus following pilocarpine-induced seizures. *Journal of Comparative Neurology* 459: 407–425.
4. Chauvière L, Rafrafi N, Thinus-Blanc C, Bartolomei F, Esclapez M, Bernard C (2009): Early Deficits in Spatial Memory and Theta Rhythm in Experimental Temporal Lobe Epilepsy. *J Neurosci* 29: 5402–5410.
5. Cossart R, Dinocourt C, Hirsch JC, Merchan-Perez A, De Felipe J, Ben-Ari Y, *et al.* (2001): Dendritic but not somatic GABAergic inhibition is decreased in experimental epilepsy. *Nature Neuroscience* 4: 52–62.
6. Dugladze T, Vida I, Tort AB, Gross A, Otahal J, Heinemann U, *et al.* (2007): Impaired hippocampal rhythmogenesis in a mouse model of mesial temporal lobe epilepsy. *PNAS* 104: 17530–17535.
7. Lopez-Pigozzi D, Laurent F, Brotons-Mas JR, Valderrama M, Valero M, Fernandez-Lamo I, *et al.* (2016): Altered Oscillatory Dynamics of CA1 Parvalbumin Basket Cells during Theta–Gamma Rhythmopathies of Temporal Lobe Epilepsy. *eneuro* 3: ENEURO.0284-16.2016.
8. Peng Z, Zhang N, Wei W, Huang CS, Cetina Y, Otis TS, Houser CR (2013): A Reorganized GABAergic Circuit in a Model of Epilepsy: Evidence from Optogenetic Labeling and Stimulation of Somatostatin Interneurons. *J Neurosci* 33: 14392–14405.

9. Proddutur A, Nguyen S, Yeh C-W, Gupta A, Santhakumar V (2023): RECLUSIVE CHANDELIERS: FUNCTIONAL ISOLATION OF DENTATE AXO-AXONIC CELLS AFTER EXPERIMENTAL STATUS EPILEPTICUS. *Prog Neurobiol* 231: 102542.

10. Wick ZC, Leintz CH, Xamonthiene C, Huang BH, Krook-Magnuson E (2017): Axonal sprouting in commissurally projecting parvalbumin-expressing interneurons. *Journal of neuroscience research* 95: 2336.

11. Lentini C, d'Orange M, Marichal N, Trottmann M-M, Vignoles R, Foucault L, *et al.* (2021): Reprogramming reactive glia into interneurons reduces chronic seizure activity in a mouse model of mesial temporal lobe epilepsy. *Cell Stem Cell* 28: 2104-2121.e10.

12. Bershteyn M, Bröer S, Parekh M, Maury Y, Havlicek S, Kriks S, *et al.* (2023): Human pallial MGE-type GABAergic interneuron cell therapy for chronic focal epilepsy. *Cell Stem Cell* 30: 1331-1350.e11.

13. Shuman T, Aharoni D, Cai DJ, Lee CR, Chavlis S, Page-Harley L, *et al.* (2020): Breakdown of spatial coding and interneuron synchronization in epileptic mice. *Nat Neurosci* 1–10.

14. Lehner A, Hoffmann L, Rampp S, Coras R, Paulsen F, Frischknecht R, *et al.* (2024): Age-dependent increase of perineuronal nets in the human hippocampus and precocious aging in epilepsy. *Epilepsia Open* n/a. https://doi.org/10.1002/epi4.12963

15. Krook-Magnuson E, Armstrong C, Oijala M, Soltesz I (2013): On-demand optogenetic control of spontaneous seizures in temporal lobe epilepsy. *Nature Communications* 4. https://doi.org/10.1038/ncomms2376

16. Lévesque M, Chen L-Y, Etter G, Shiri Z, Wang S, Williams S, Avoli M (2019): Paradoxical effects of optogenetic stimulation in mesial temporal lobe epilepsy. *Annals of Neurology* 86: 714–728.

17. Wang Y, Wang Y, Xu C, Wang S, Tan N, Chen C, *et al.* (2020): Direct Septum-Hippocampus Cholinergic Circuit Attenuates Seizure Through Driving Somatostatin Inhibition. *Biological Psychiatry* 87: 843–856.

18. Kim HK, Gschwind T, Nguyen TM, Bui AD, Felong S, Ampig K, *et al.* (2020): Optogenetic intervention of seizures improves spatial memory in a mouse model of chronic temporal lobe epilepsy. *Epilepsia*. https://doi.org/10.1111/epi.16445

19. Wang Y, Liang J, Chen L, Shen Y, Zhao J, Xu C, *et al.* (2018): Pharmaco-genetic therapeutics targeting parvalbumin neurons attenuate temporal lobe epilepsy. *Neurobiology of Disease* 117: 149–160.

20. Amilhon B, Huh CYL, Manseau F, Ducharme G, Nichol H, Adamantidis A, Williams S (2015): Parvalbumin Interneurons of Hippocampus Tune Population Activity at Theta Frequency. *Neuron* 86: 1277–1289.

21. Dudok B, Klein PM, Soltesz I (2022): Toward Understanding the Diverse Roles of Perisomatic Interneurons in Epilepsy. *Epilepsy Curr* 22: 54–60.

22. Dudok B, Klein PM, Hwaun E, Lee BR, Yao Z, Fong O, *et al.* (2021): Alternating sources of perisomatic inhibition during behavior. *Neuron* 109: 997-1012.e9.

23. Miri ML, Vinck M, Pant R, Cardin JA (2018): Altered hippocampal interneuron activity precedes ictal onset ((G. L. Westbrook & C. Schevon, editors)). *eLife* 7: e40750.

24. Parrish RR, Codadu NK, Scott CM-G, Trevelyan AJ (2019): Feedforward inhibition ahead of ictal wavefronts is provided by both parvalbumin- and somatostatin-expressing interneurons. *The Journal of Physiology* 597: 2297–2314.

25. Bocchio M, Vorobyev A, Sadeh S, Brustlein S, Dard R, Reichinnek S, *et al.* (2023, September 18): Functional networks of inhibitory neurons orchestrate synchrony in the hippocampus. bioRxiv, p 2023.09.18.558335.

26. Ledri M, Madsen MG, Nikitidou L, Kirik D, Kokaia M (2014): Global Optogenetic Activation of Inhibitory Interneurons during Epileptiform Activity. *J Neurosci* 34: 3364–3377.

27. Vigier A, Partouche N, Michel FJ, Crépel V, Marissal T (2021): Substantial outcome improvement using a refined pilocarpine mouse model of temporal lobe epilepsy. *Neurobiology of Disease* 161: 105547.

28. Goirand-Lopez L, Moulinier M, Vigier A, Boileau C, Carleton A, Muldoon SF, *et al.* (2023): Kainate receptors modulate the microstructure of synchrony during dentate gyrus epileptiform activity. *Neurobiology of Disease* 185: 106260.

29. Boileau C, Deforges S, Peret A, Scavarda D, Bartolomei F, Giles A, *et al.* (2023): GluK2 Is a Target for Gene Therapy in Drug-Resistant Temporal Lobe Epilepsy. *Annals of Neurology* 94: 745–761.

30. Călin A, Stancu M, Zagrean A-M, Jefferys JGR, Ilie AS, Akerman CJ (2018): Chemogenetic Recruitment of Specific Interneurons Suppresses Seizure Activity. *Frontiers in Cellular Neuroscience* 12. https://doi.org/10.3389/fncel.2018.00293

31. Peret A, Christie LA, Ouedraogo DW, Gorlewicz A, Epsztein J, Mulle C, Crépel V (2014): Contribution of Aberrant GluK2-Containing Kainate Receptors to Chronic Seizures in Temporal Lobe Epilepsy. *Cell Reports* 8: 347–354.

32. Dimidschstein J, Chen Q, Tremblay R, Rogers SL, Saldi G-A, Guo L, *et al.* (2016): A viral strategy for targeting and manipulating interneurons across vertebrate species. *Nature Neuroscience* 19: 1743–1749.

33. Zhan J, Komal R, Keenan WT, Hattar S, Fernandez DC (2019): Non-invasive Strategies for Chronic Manipulation of DREADD-controlled Neuronal Activity. *J Vis Exp* 10.3791/59439.

34. Milosavljevic N, Cehajic-Kapetanovic J, Procyk CA, Lucas RJ (2016): Chemogenetic Activation of Melanopsin Retinal Ganglion Cells Induces Signatures of Arousal and/or Anxiety in Mice. *Current Biology* 26: 2358–2363.

35. Gawel K, Gibula E, Marszalek-Grabska M, Filarowska J, Kotlinska JH (2019): Assessment of spatial learning and memory in the Barnes maze task in rodents—methodological consideration. *Naunyn-Schmiedeberg's Archives of Pharmacology* 392: 1.

36. Carola V, D'Olimpio F, Brunamonti E, Mangia F, Renzi P (2002): Evaluation of the elevated plus-maze and open-field tests for the assessment of anxiety-related behaviour in inbred mice. *Behavioural Brain Research* 134: 49–57.

37. Antunes M, Biala G (2012): The novel object recognition memory: neurobiology, test procedure, and its modifications. *Cogn Process* 13: 93–110.

38. Cohen SJ, Munchow AH, Rios LM, Zhang G, Ásgeirsdóttir HN, Stackman RW (2013): The Rodent Hippocampus Is Essential for Nonspatial Object Memory. *Current Biology* 23: 1685–1690.

39. Zhang Y, Rózsa M, Liang Y, Bushey D, Wei Z, Zheng J, *et al.* (2023): Fast and sensitive GCaMP calcium indicators for imaging neural populations [no. 7954]. *Nature* 615: 884–891.

40. Li P, Geng X, Jiang H, Caccavano A, Vicini S, Wu J (2019): Measuring Sharp Waves and Oscillatory Population Activity With the Genetically Encoded Calcium Indicator GCaMP6f. *Frontiers in Cellular Neuroscience* 13. Retrieved January 10, 2023, from https://www.frontiersin.org/articles/10.3389/fncel.2019.00274

41. Marissal T, Salazar RF, Bertollini C, Mutel S, De Roo M, Rodriguez I, *et al.* (2018): Restoring wild-type-like CA1 network dynamics and behavior during adulthood in a mouse model of schizophrenia. *Nature Neuroscience* 21: 1412–1420.

42. Fisahn A, Pike FG, Buhl EH, Paulsen O (1998): Cholinergic induction of network oscillations at 40 Hz in the hippocampus in vitro. *Nature* 394: 186–189.

43. Lim J-A, Moon J, Kim T-J, Jun J-S, Park B, Byun J-I, *et al.* (2018): Clustering of spontaneous recurrent seizures separated by long seizure-free periods: An extended video-EEG monitoring study of a pilocarpine mouse model. *PLOS ONE* 13: e0194552.

44. Padmasola GP, Friscourt F, Rigoni I, Vulliémoz S, Schaller K, Michel CM, *et al.* (2024): Involvement of the contralateral hippocampus in ictal-like but not interictal epileptic activities in the kainate mouse model of temporal lobe epilepsy. *Epilepsia*. https://doi.org/10.1111/epi.17970

45. Brewster AL, Lugo JN, Patil VV, Lee WL, Qian Y, Vanegas F, Anderson AE (2013): Rapamycin Reverses Status Epilepticus-Induced Memory Deficits and Dendritic Damage. *PLOS ONE* 8: e57808.

46. Bernard C, Esclapez M, Hirsch JC, Ben-Ari Y (1998): Interneurones are not so dormant in temporal lobe epilepsy: a critical reappraisal of the dormant basket cell hypothesis. *Epilepsy Research* 32: 93–103.

47. Dugladze T, Vida I, Tort AB, Gross A, Otahal J, Heinemann U, *et al.* (2007): Impaired hippocampal rhythmogenesis in a mouse model of mesial temporal lobe epilepsy. *Proceedings of the National Academy of Sciences* 104: 17530–17535.

48. Sloviter RS (1987): Decreased Hippocampal Inhibition and a Selective Loss of Interneurons in Experimental Epilepsy. *Science* 235: 73–76.

49. Toyoda I, Bower MR, Leyva F, Buckmaster PS (2013): Early activation of ventral hippocampus and subiculum during spontaneous seizures in a rat model of temporal lobe epilepsy. *J Neurosci* 33: 11100–11115.

50. Gröticke I, Hoffmann K, Löscher W (2007): Behavioral alterations in the pilocarpine model of temporal lobe epilepsy in mice [no. 2]. *Experimental Neurology* 207: 329–349.

51. Lenck-Santini P-P, Holmes GL (2008): Altered Phase Precession and Compression of Temporal Sequences by Place Cells in Epileptic Rats. *J Neurosci* 28: 5053–5062.

52. Arriaga M, Han EB (2017): Dedicated Hippocampal Inhibitory Networks for Locomotion and Immobility. *J Neurosci* 37: 9222–9238.

53. Jimenez JC, Su K, Goldberg AR, Luna VM, Biane JS, Ordek G, *et al.* (2018): Anxiety Cells in a Hippocampal-Hypothalamic Circuit. *Neuron* 97: 670-683.e6.

54. Ang CW, Carlson GC, Coulter DA (2006): Massive and Specific Dysregulation of Direct Cortical Input to the Hippocampus in Temporal Lobe Epilepsy. *J Neurosci* 26: 11850–11856.

55. Buckmaster PS, Reyes B, Kahn T, Wyeth M (2022): Ventral Hippocampal Formation Is the Primary Epileptogenic Zone in a Rat Model of Temporal Lobe Epilepsy. *J Neurosci* 42: 7482–7495.

56. Wozny C, Gabriel S, Jandova K, Schulze K, Heinemann U, Behr J (2005): Entorhinal cortex entrains epileptiform activity in CA1 in pilocarpine-treated rats. *Neurobiology of Disease* 19: 451–460.

57. Kahn JB, Port RG, Yue C, Takano H, Coulter DA (2019): Circuit-based interventions in the dentate gyrus rescue epilepsy-associated cognitive dysfunction. *Brain* 142: 2705–2721.

58. Klausberger T, Somogyi P (2008): Neuronal Diversity and Temporal Dynamics: The Unity of Hippocampal Circuit Operations. *Science* 321: 53–57.

59. Muldoon SF, Villette V, Tressard T, Malvache A, Reichinnek S, Bartolomei F, Cossart R (2015): GABAergic inhibition shapes interictal dynamics in awake epileptic mice. *Brain* 138: 2875–2890.

60. Ling Q, Herstine JA, Bradbury A, Gray SJ (2023): AAV-based in vivo gene therapy for neurological disorders. *Nat Rev Drug Discov* 22: 789–806.

61. Marissal T (2021): An inventory of basic research in temporal lobe epilepsy. *Revue Neurologique*.

62. Ewell LA, Fischer KB, Leibold C, Leutgeb S, Leutgeb JK (2019): The impact of pathological high-frequency oscillations on hippocampal network activity in rats with chronic epilepsy ((J. Huguenard & L. Colgin, editors)). *eLife* 8: e42148.

63. Qiu Y, O'Neill N, Maffei B, Zourray C, Almacellas-Barbanoj A, Carpenter JC, *et al.* (2022): On-demand cell-autonomous gene therapy for brain circuit disorders. *Science* 378: 523–532.

Figure Legends

Figure 1: Epileptic mice display impaired behavior related to spatial learning and memory, but no loss of CA1 inhibitory neurons. A. Schematic representation of the BCM acquisition phase and pie charts showing the cumulated percentage of non-epileptic animals ("Controls") or pilocarpine-treated chronically epileptic mice ("Pilo") that found (success) or not (failure) the escape room at least once during the different days of the acquisition phase. The number of mice succeeding or failing to find the escape room at least once in each step and experimental condition was compared using Fisher's exact test. **B.** Schematic representation of the BCM probe trial and pie charts indicating the cumulated percentage of Controls or Pilo mice that found (success) or not (failure) the former location of the escape room during the probe trial. The number of mice succeeding or failing to find the previous location of the escape room was compared using Fisher's exact test. **C.** Min-max scores of latencies to find the escape room during the different BCM phases (two-way repeated measures ANOVA: experimental group effect F (1, 33) = 24.45, followed by Sidak's post hoc test, p = 0.0066, 0.2810, 0.0029, 0.0526 and 0.0386 for days 1-4 and PT). **D.** Min-max scores of numbers of primary errors, i.e., number of incorrect holes checked prior to identifying the escape room location or the completion of the test (two-way repeated measures ANOVA: experimental group effect F (1, 33) = 15,91 followed by Sidak's post hoc test, p = 0.1507, 0.5454, 0.1020, 0.2607 and 0.0461 for days 1-4 and PT). **E.** Min-max scores of times spent in the target zone (Two-tailed Mann-Whitney test). **F.** Representative Hoechst staining (left), as well as PV (middle) and SOM (right) immunolabelling from a control (top) or a Pilo (bottom) mouse. SO: Stratum Oriens, SP: stratum Pyramidale, SR: Stratum Radiatum. **G-H.** Number of Parvalbumin- (PV, J) and Somatostatin- (SOM, K) expressing interneurons per mm^2 of CA1 (Two-tailed Mann-Whitney test, p = 0.1061 and 0.8763, respectively). Asterisks indicate significant differences ($p < 0.05$). The number of mice is specified in parentheses. Unless indicated otherwise, data are presented as mean ± s.e.m. Each circle or line represents a given mouse. C-E: The data is scaled using a min-max normalization (see Methods and Materials and Figure S1 for the original data).

Figure 2: Epileptic CA1 network is hyperactive and synchronous and inhibitory neurons are less active. A. Schematic representation of the experimental procedure and photograph of GCaMP8m-expressing neurons in the hippocampal CA1 region. SO: Stratum Oriens, SP: Stratum Pyramidale, SR: Stratum Radiatum. **B.** Contours (B) of GCaMP8m-expressing neurons shown in A. **C.** Calcium transients recorded in the presence of carbachol (50 µM) from selected neurons identified as 1 to 5 in B (represented with red-filled contours). **D-E.** Representative raster plots of calcium transients recorded in control (D, black) or Pilo (E, red) conditions. **F.** Proportion of CA1 neurons displaying at least one calcium transient during the duration of the movie in each condition (Two-tailed unpaired t-test, p = 0,3748). **G.** Frequency of calcium transients recorded in all CA1 neurons (Two-tailed Mann-Whitney test). **H-I.** Percentage of co-active neurons above chance level (H) and occurrence (I) of these co-activations (Two-tailed Mann-Whitney test). **J.** Photograph of the field represented by a dashed rectangle in A, in which an interneuron co-express GCaMP8m and dTomato. **K**. Number of interneurons per calcium imaging field (Two-tailed Mann-Whitney test, p = 0,5879). **L.** Example of calcium activity exhibited by interneurons in control (left) or pilo (right) conditions. **M.** Frequency of calcium transients recorded in CA1 interneurons (Two-tailed Mann-Whitney test). Asterisks indicate significant differences ($p < 0.05$). Data are presented as mean ± s.e.m. Each circle represents the mean for a given slice (the number of slices is specified in parentheses. Slices were prepared from N = 4 and 5 animals in control and pilo conditions, respectively).

Figure 3: Reestablishing interneuron activity decreases local CA1 network synchronization. A. Photograph of CA1 interneurons that co-express GCaMP8m and dTomato (fused to hm3D) and example of calcium activity exhibited by hm3D-expressing CA1 interneurons in Pilo condition before (red, Pilo-VEH) and after 15 minutes of treatment with CNO (2 µM). **B.** Frequency of calcium transients recorded in hm3D-expressing CA1 interneurons in Pilo condition before and after treatment with CNO (Two-tailed Wilcoxon test). **C.** Representative raster plots of calcium transients recorded in the same slice before and after treatment with CNO. **D-G.** Levels of calcium activity (D, E) and synchronization (F, G) in both conditions (Two-tailed paired t-test for D and E, Two-tailed Wilcoxon test for F and G). Data are presented as mean ± s.e.m. Each gray line represents a given slice (the number of slices is specified in parentheses. Slices were prepared from N = 3 animals in pilo condition).

Figure 4: The chemoactivation of interneurons reduces the behavioral deficits in epileptic mice, but not generalized seizures.
A. Schematic representation of the experimental procedure and example traces of ictal activity recorded with telemetric EEG recording in freely moving epileptic mice in the absence (Pilo-VEH) or presence of CNO (Pilo-CNO) in the drinking water to specifically elevate or not the activity of hm3D-expressing hippocampal interneurons. **B-C.** Frequency (B) and duration (C) of ictal events in Pilo-VEH versus Pilo-CNO conditions (Two-tailed paired t-test, p = 0,1170 for B, p = 0,9895 for C). **D-E.** Pie charts showing the percentage of mice that found (success) or not (failure) the location of the escape room at least once during the different days of the BCM acquisition phase (D), or during the probe trial (E). Data are plotted for mice from the following experimental conditions: control mice treated with vehicle (control-VEH) and epileptic mice treated with vehicle (pilo-VEH) or CNO (pilo-VEH) to specifically elevate or not the activity of hm3D-expressing hippocampal interneurons. The number of mice succeeding or failing to find the escape room at least once in each step and experimental condition was compared using Fisher's exact test. **F.** Min-max scores of latencies to find the escape room during the BCM acquisition phase. Data were compared in Control-VEH versus Pilo-VEH groups (Two-way ANOVA experimental group effect F (1, 32) = 24.82 p < 0.0001, followed by Sidak's post hoc test, p = 0.0001, 0.0001, 0.0001, 0.007 and 0.0009 for days 1-4 and PT), Control-VEH versus Pilo-CNO groups (Two-way ANOVA experimental group and treatment effect F (1, 25) = 35.20 p < 0.001, followed by Sidak's post hoc test, p = 0.001, 0.0003, 0.0014, 0.0510 and 0.0527 for days 1-4 and PT), and Pilo-VEH versus Pilo-CNO groups (Two-way ANOVA treatment effect F (1, 37) = 0.09, p = 0.7585). **G.** Min-max scores of the number of incorrect holes checked prior to identifying the escape room or the completion of the test, in each experimental conditions Data were compared in Control-VEH versus Pilo-VEH groups (Two-way ANOVA experimental group effect F (1, 32) = 16.79 p = 0.003, followed by Sidak's post hoc test, p = 0.0031, 0.0054, 0.0012, 0.0218 and 0.0004 for days 1-4 and PT), Control-VEH versus Pilo-CNO groups (Two-way ANOVA experimental group and treatment effect F (1, 25) = 20.08, p = 0.0001, followed by Sidak's post hoc test, p = 0.0287, 0.0840, 0.1717, 0.1566 and 0.1856 for days 1-4 and PT), and Pilo-VEH versus Pilo-CNO groups (Two-way ANOVA treatment effect F (1, 37) = 1.307, p = 0.2603). **H.** Min-max scores of times spent in the target zone during the BCM probe trial in various experimental conditions (Two-tailed Mann-Whitney test for the comparison between Control-VEH and Pilo-VEH and between Pilo-VEH and Pilo-CNO, unpaired t-test for the comparison between control-VEH and Pilo-CNO, p = 0.1329). **I.** Schematic representation of the NORT procedure. **J.** Time spent exploring the novel and the familiar object during the NORT test phase, in each experimental condition (two-way ANOVA interaction experimental condition x type of object F (2, 45) = 8.182, p = 0.009). Asterisks indicate significant differences with the Control-VEH condition (p < 0.05), unless specified otherwise. Data are presented as mean ± s.e.m, unless specified otherwise. Each circle or line represents a given mouse (The number of mice is specified in parentheses).

Figure 1

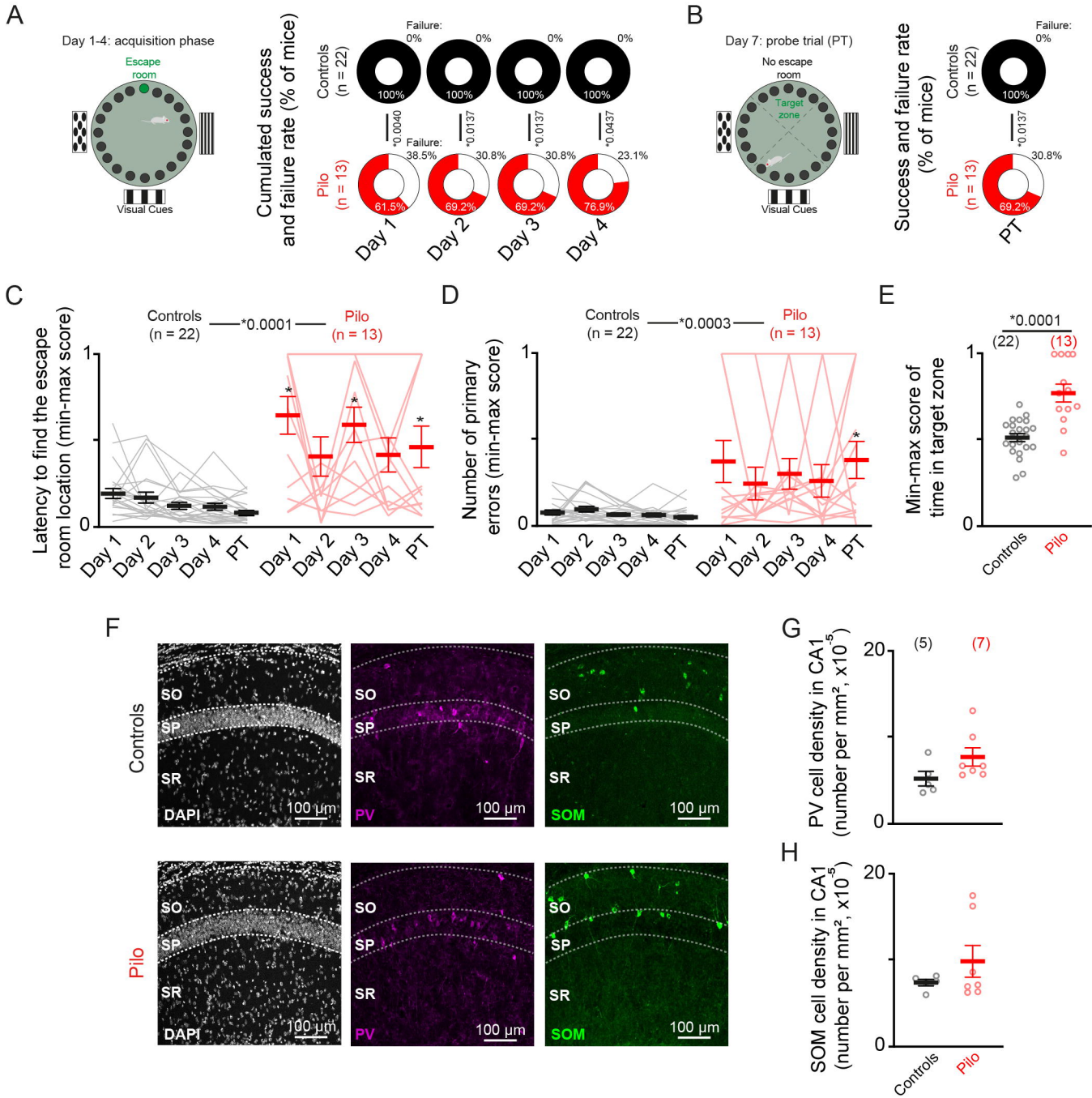
A
Day 1-4: acquisition phase
Escape room
Visual Cues
Cumulated success and failure rate (% of mice)
Controls (n = 22)
Failure: 0%
100%
*0.0040
*0.0137
*0.0437
Pilo (n = 13)
38.5%
30.8%
23.1%
61.5%
69.2%
76.9%
Day 1
Day 2
Day 3
Day 4
B
Day 7: probe trial (PT)
No escape room
Target zone
Visual Cues
Success and failure rate (% of mice)
PT
C
Controls (n = 22)
*0.0001
Pilo (n = 13)
Latency to find the escape room location (min-max score)
Day 1
Day 2
Day 3
Day 4
PT
D
*0.0003
Number of primary errors (min-max score)
E
*0.0001
(22)
(13)
Min-max score of time in target zone
Controls
Pilo
F
Controls
Pilo
SO
SP
SR
DAPI
PV
SOM
100 µm
G
(5)
(7)
PV cell density in CA1 (number per mm², x10⁻⁵)
H
SOM cell density in CA1 (number per mm², x10⁻⁵)

Figure 2

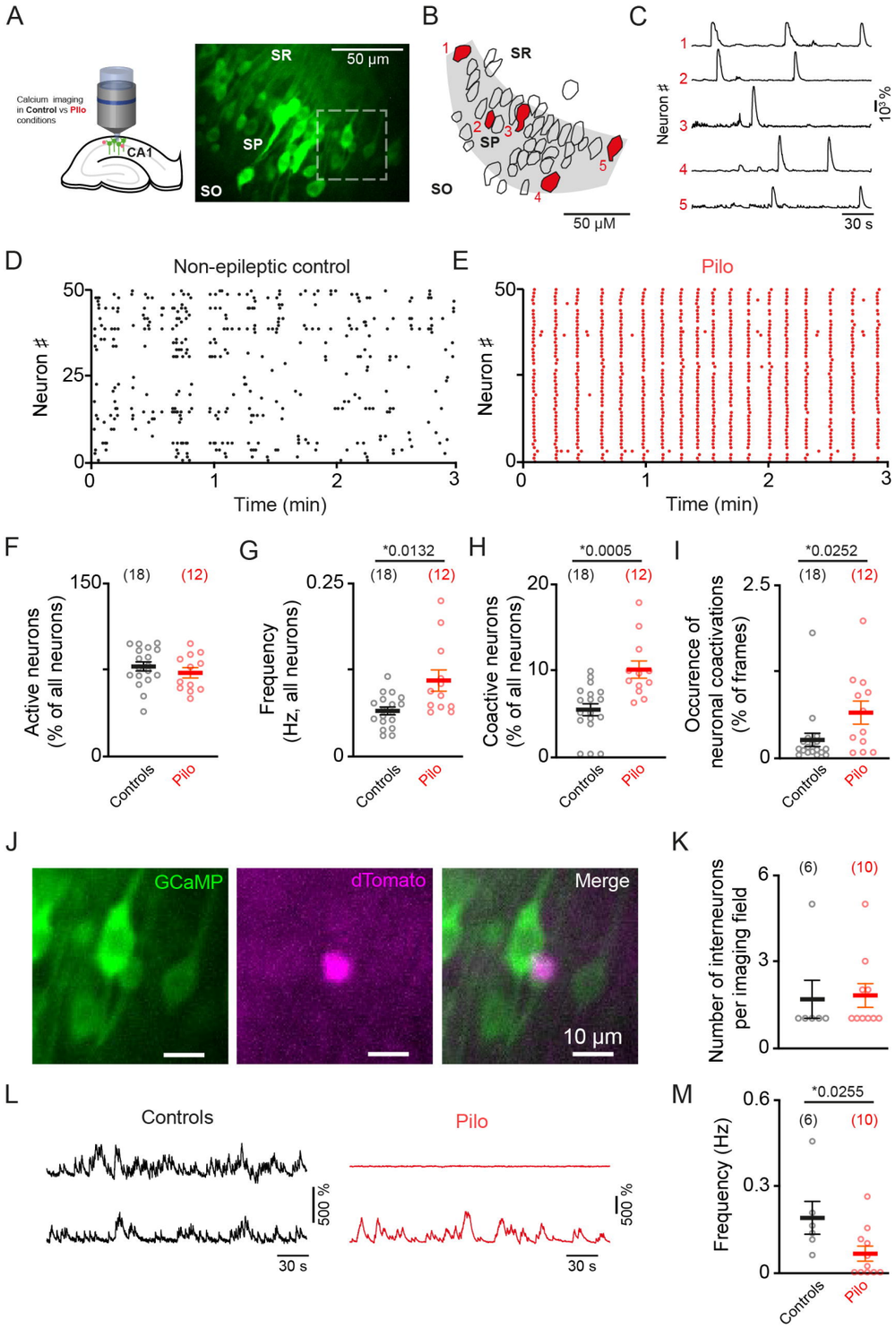
A
Calcium imaging in Control vs Pilo conditions
CA1
SR
50 µm
SP
SO
B
SR
SP
SO
50 µM
C
Neuron #
10 %
30 s
D
Non-epileptic control
Neuron #
Time (min)
E
Pilo
Neuron #
Time (min)
F
Active neurons (% of all neurons)
(18)
(12)
Controls
Pilo
G
*0.0132
Frequency (Hz, all neurons)
H
*0.0005
Coactive neurons (% of all neurons)
I
*0.0252
Occurence of neuronal coactivations (% of frames)
J
GCaMP
dTomato
Merge
10 µm
K
Number of interneurons per imaging field
(6)
(10)
L
Controls
Pilo
500 %
30 s
M
*0.0255
Frequency (Hz)

Figure 3

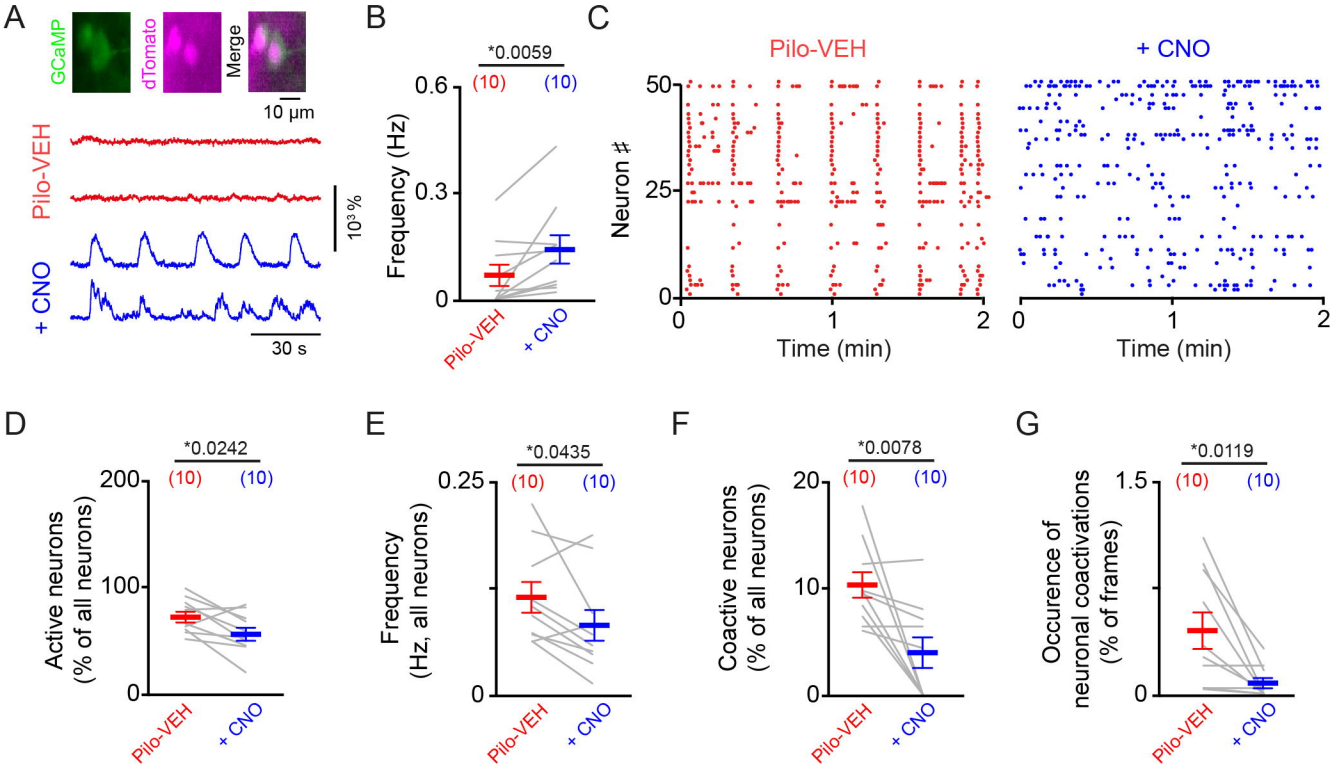
A
GCaMP
dTomato
Merge
10 µm
Pilo-VEH
+ CNO
10³ %
30 s
B
*0.0059
(10)
(10)
Frequency (Hz)
0.6
0.3
0
Pilo-VEH
+ CNO
C
Pilo-VEH
+ CNO
Neuron #
50
25
0
0
1
2
Time (min)
D
*0.0242
Active neurons
(% of all neurons)
200
100
0
E
*0.0435
Frequency
(Hz, all neurons)
0.25
0
F
*0.0078
Coactive neurons
(% of all neurons)
20
10
0
G
*0.0119
Occurence of
neuronal coactivations
(% of frames)
1.5
0

Figure 4

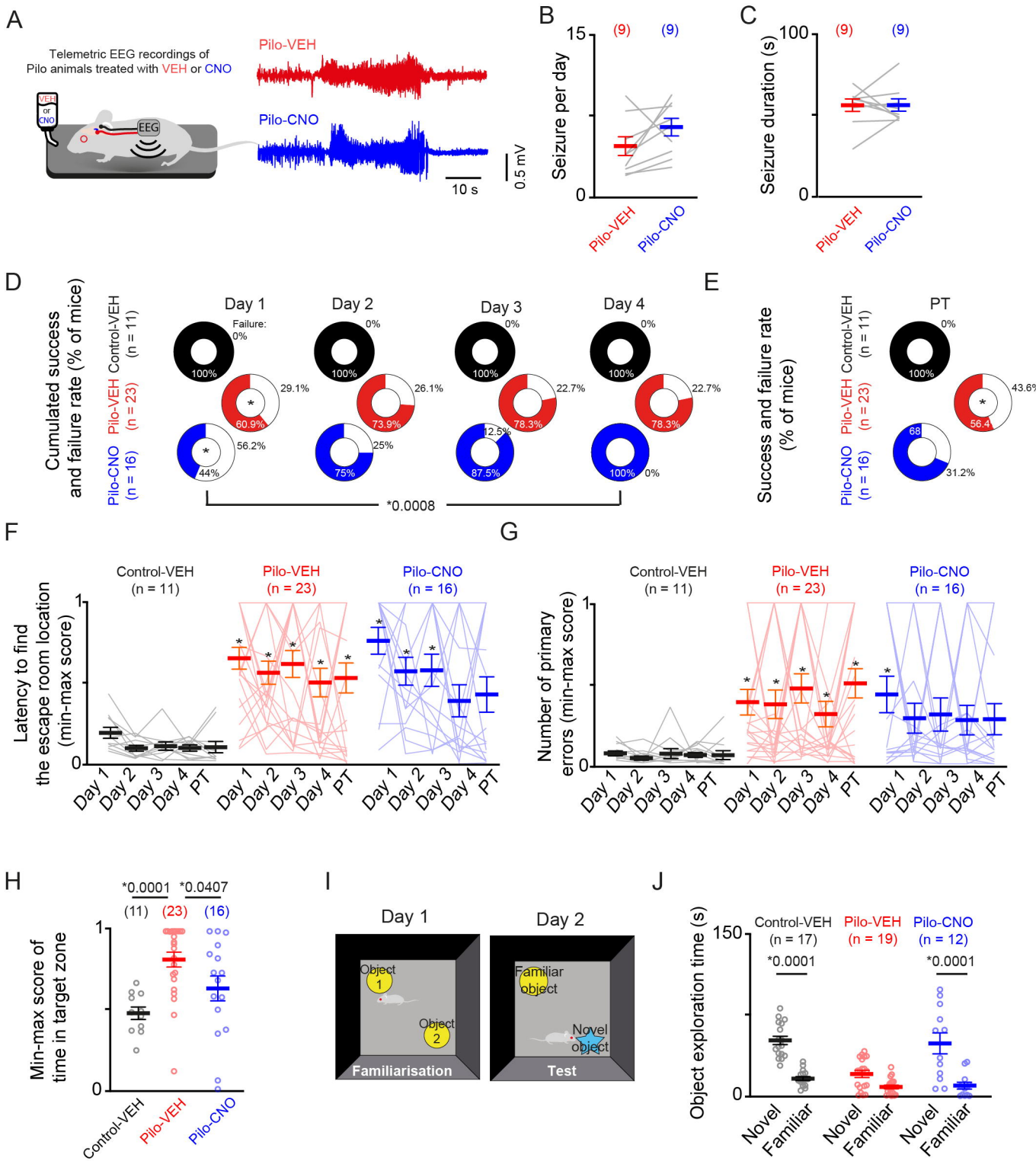
A
Telemetric EEG recordings of
Pilo animals treated with VEH or CNO
VEH or CNO
EEG
Pilo-VEH
Pilo-CNO
10 s
0.5 mV
B
Seizure per day
(9)
(9)
Pilo-VEH
Pilo-CNO
C
Seizure duration (s)
(9)
(9)
Pilo-VEH
Pilo-CNO
D
Cumulated success and failure rate (% of mice)
Control-VEH (n = 11)
Pilo-VEH (n = 23)
Pilo-CNO (n = 16)
Day 1
Day 2
Day 3
Day 4
Failure: 0%
100%
29.1%
60.9%
56.2%
44%
26.1%
73.9%
25%
75%
22.7%
78.3%
12.5%
87.5%
*0.0008
E
Success and failure rate (% of mice)
PT
43.6%
56.4
68
31.2%
F
Latency to find the escape room location (min-max score)
Control-VEH (n = 11)
Pilo-VEH (n = 23)
Pilo-CNO (n = 16)
Day 1
Day 2
Day 3
Day 4
PT
G
Number of primary errors (min-max score)
H
Min-max score of time in target zone
*0.0001
*0.0407
(11)
(23)
(16)
Control-VEH
Pilo-VEH
Pilo-CNO
I
Day 1
Day 2
Object 1
Object 2
Familiarisation
Familiar object
Novel object
Test
J
Object exploration time (s)
Control-VEH (n = 17)
Pilo-VEH (n = 19)
Pilo-CNO (n = 12)
*0.0001
*0.0001
Novel
Familiar